2016 23rd International Conference on Pattern Recognition (ICPR)
Cancún Center, Cancún, México, December 4-8, 2016

Learning-Based Single Image Dehazing via Genetic Programming

Chulwoo Lee and Ling Shao
Department of Computer and Information Sciences, Northumbria University, UK
chulwoo.lee@outlook.com and ling.shao@ieee.org

***Abstract*—A genetic programming (GP)-based framework to learn the effective feature representation for image dehazing is proposed in this work. In GP, an individual program is randomly generated and genetically evolved to achieve the desired goal. To make GP estimate haze in an input image, a set of operators and operands is designed, each of which is a primitive of a GP program. Specifically, we provide four basic features as candidates, and also include function operators to construct sophisticated representations of these features. After the entire GP process finishes, we obtain a near-optimal compact descriptor for haze estimation. Experimental results demonstrate that the proposed algorithm enhances the visual quality of haze-degraded images both objectively and subjectively.**

I. Introduction

Even though recent advances in imaging technologies make it easier to capture scene details faithfully, we often acquire low contrast images with severe information loss. Especially in the outdoor environment, a turbid medium such as fog, dust and smoke causes poor visual perception to viewers and decreases recognition accuracy in many vision applications. Therefore, haze removal, equivalently dehazing, has been actively studied in the recent decade.

In the early development of dehazing, a variety of attempts has been made to find effective methods. However, due to a large number of unknowns, researchers have tried to solve the problem by exploiting additional information, e.g. captured scenes under different weather conditions [1], two or more polarization-filtered images [2], near-infrared (NIR) light imaging [3], and public 3D geometric models of the scene [4]. While these approaches can improve the visibility, their requirements are too strict to deliver their results immediately. To capture meaningful data, both camera and subject should be prepared in a certain condition between successive acquisitions. To overcome this limitation, dehazing algorithms that only require a single input image have drawn much attention.

Single image haze removal, however, still suffers from many unknown variables, and hence a strong assumption or prior knowledge is required to solve the ill-posed problem. Narashimhan and Nayar [5] and Hautiére et al. [6] addressed the image dehazing problem by approximating specific types of 3D structures that frequently appear in the urban scene, e.g. perspective landscape and road view observed in a moving vehicle. Desirable conditions for recovered scene radiance and the locally independent relationship between haze and image contents are often used for haze removal. Tan [7] attempted to enhance the visibility of hazy images by maximizing contrast of local patches. Fattal [8] assumed that the medium transmission and surface shading are locally uncorrelated and then estimated the haze by independent component analysis. He et al. [9] proposed a single image dehazing algorithm based on the observation that at least one color channel has some pixels whose intensity values are very low and close to zero in most of the non-sky patches. This assumption, called dark channel prior (DCP), is simple and effective and thus it has been employed to various dehazing applications.

Recently, machine learning techniques allow more accurate and faster implementation of image processing and computer vision tasks. By taking advantage of machine learning and principle of the atmospheric scattering, several approaches have been developed for dehazing. Gibson et al. [10] have tried to estimate the medium transmission by applying an example-based learning framework [11] originally proposed for super-resolution. Tang et al. [12] proposed a data-driven approach to investigate haze-relevant features using Random Forest [13]. Zhu et al. [14] modeled pixel-wise scene depth as a linear combination of HSV color components and learned parameters of the model by least squares regression.

As an alternative machine learning framework, genetic programming (GP), a powerful evolutionary process inspired by natural phenomenon, can be employed to discover haze in the scene. In image dehazing, we attempt to find an effective haze estimator by combining various features. GP has demonstrated its ability to extract meaningful information from input data. For example, Poli [15] applied GP to select an optimal filter for segmentation in medical imaging. Torres et al. [16] used GP to find a combination of similarity functions for image retrieval. Davis et al. [17] have also employed GP for discriminative feature selection in multivariate data analysis. More recently, Liu et al. [18] exploited GP to learn the spatiotemporal representation of visual features for human action recognition [18].

Inspired by the effectiveness of GP on various learning tasks, we use it to discover a robust feature representation for haze removal. To this end, we first design low-level

This research was supported by Basic Science Research Program through the National Research Foundation of Korea (NRF) funded by the Ministry of Education (2015R1A6A3A03020215)

978-1-5090-4847-2/16/$31.00 ©2016 IEEE

features and operators to extract haze components from an input image. Based on a set of primitives, GP builds an initial population of individual programs and evolves them generation by generation to fit their programs to the ground-truth data. From the output of GP, we obtain a compact representation of haze features. Specifically, we verify that the physical boundary of medium transmission gives strong prior knowledge for haze estimation. Experimental results demonstrate that the proposed algorithm improves dehazing performance significantly, compared with recent state-of-the-art dehazing techniques [9], [14], [19]–[21], on real-world datasets.

The rest of this paper is organized as follows: Section II reviews the background related to this work. Section III proposes the GP architecture for dehazing. Section IV explains scene radiance recovery from the learned model, and Section V presents experimental results. Section VI concludes this work.

II. Background

In this section, we briefly introduce the principle of atmospheric scattering for dehazing and explain the basic of GP on which the proposed approach is based.

A. Atmospheric Scattering Model

From the physical model in [22], [23], image degradation by atmospheric scattering is formulated as

$$\mathbf{I}(\mathbf{x}) = \mathbf{J}(\mathbf{x})t(\mathbf{x}) + (1 - t(\mathbf{x}))\,\mathbf{A}, \tag{1}$$

where $\mathbf{J}(\mathbf{x})$ and $\mathbf{I}(\mathbf{x})$ are the original and degraded RGB color vectors at pixel coordinate $\mathbf{x}$, respectively, and $\mathbf{A}$ denotes an atmospheric light color in RGB space. Also, transmission $t(\mathbf{x})$ quantifies an ability of atmosphere that can deliver the light intensity without attenuation. Since it is mainly affected by the distance between the scene point and the camera, $t(\mathbf{x}) = \exp(-\beta d(\mathbf{x}))$, where $d(\mathbf{x})$ is the scene depth and β is the scattering coefficient of the atmosphere.

According to the atmospheric scattering model (1), the scene radiance $\mathbf{J}$ is degraded by spatially varying transmission t. Therefore, robust estimation of the transmission t is the main objective of haze removal, which we tackle in this paper. To reduce the number of degrees of freedom in (1), we assume that $\mathbf{A}$ is given in the learning phase. We refer the reader to [24] for sophisticated estimation of $\mathbf{A}$.

B. Genetic Programming

GP is an evolutionary computation technique that automatically solves problems without requiring the user to know or specify the form or structure of the solution in advance [25]. The general procedure of GP is as follows. First, we randomly create an initial population that consists of individual programs, each of which is considered as a candidate solution. Then, GP stochastically evolves the population by genetic operations such as selection, crossover, and mutation. Underlying randomness in these operations leads it to escape local minima which deterministic methods may be captured. As generation continues, the overall population improves their fitness to the ground-truth training data. Finally, the best-so-far individual is taken as the solution. It is worth noting that GP does not guarantee the optimal solution, but it can provide a near-optimal one in an acceptable amount of computation time.

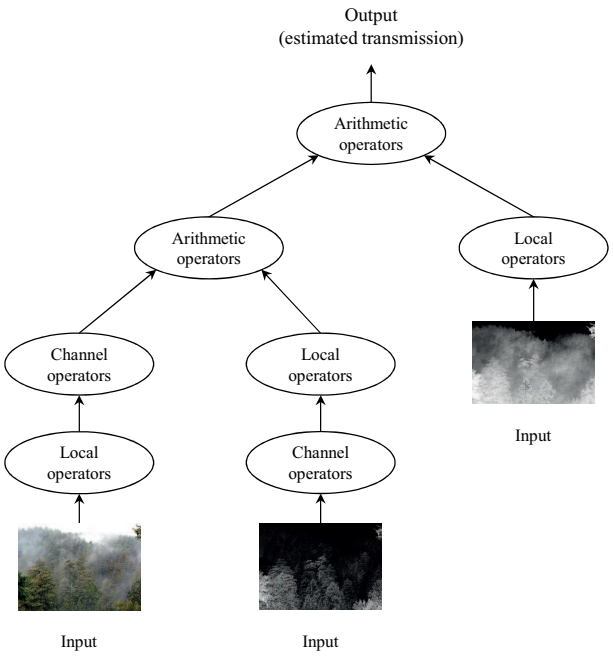

Fig. 1. An example of GP program represented in a tree structure.

In GP, an individual program in the population is represented as a tree structure, making mathematical expressions easy to evolve and evaluate. To make GP search the possible solution space efficiently, available nodes of the tree should be first defined. In our work, we design four input features and a set of function operators to describe transmission at each pixel position. Figure 1 shows an example of the GP program. Let us explain these components subsequently.

III. GP-based Feature Extraction

In this section, we construct a set of terminal nodes using well-known image features that are related to the haze. Also, a set of function operators is defined for high order feature representation, as listed in Table I.

A. Terminal Set as Input Features

A raw input image $\mathbf{I}$ is a basic ingredient for haze estimation. From the grayish region of an input image in Figure 2(a), we intuitively see that the brightness is positively related to the haze. Therefore, we include an RGB color image $\mathbf{I}$ in a terminal set. Once it is involved with functional operators, which will be explained later, it can be evolved as a well-known dark channel of an image $\mathbf{I}$.

If we know the atmospheric light vector $\mathbf{A}$, it would be beneficial for accurate estimation of transmission t. According to the atmospheric scattering model (1), transmission is

TABLE I
EXAMPLES OF PRIMITIVES IN THE PROPOSED GP.

Terminal set	Function set	
	Channel operators	Local operators
$\mathbf{I}$	$\max_{c\in\{r,g,b\}}$	$\max_{\mathbf{y}\in\mathcal{N}(\mathbf{x})}$
$\lvert\mathbf{I}-\mathbf{A}\rvert$	$\min_{c\in\{r,g,b\}}$	$\min_{\mathbf{y}\in\mathcal{N}(\mathbf{x})}$
I_{sat}	$\text{mean}_{c\in\{r,g,b\}}$	$\text{mean}_{\mathbf{y}\in\mathcal{N}(\mathbf{x})}$
I_{low}		$\text{median}_{\mathbf{y}\in\mathcal{N}(\mathbf{x})}$
		$\text{var}_{\mathbf{y}\in\mathcal{N}(\mathbf{x})}$

proportional to the difference between the input hazy scene and the atmospheric light vector, i.e. $\mathbf{I}-\mathbf{A}=(\mathbf{J}-\mathbf{A})t$. By taking absolute to avoid negative values, we have atmospheric light compensated image $|\mathbf{I}-\mathbf{A}|$ as a second input feature for our terminal set. In Figure 2(b), a certain channel of $|\mathbf{I}-\mathbf{A}|$ exhibits strong correlation with haze.

For hazy pixels with low transmission values, their color distinctiveness is significantly reduced. In this sense, image saturation, the ratio between maximum and minimum intensities of RGB values, is an important haze cue. Tang et al. [12] used locally maximum saturation to describe the amount of haze in the corresponding patches. Zhu et al. [14] employed this feature to find a linear relationship between input hazy pixels and the scene depth. We also adopt image saturation as an input feature for our framework. Figure 2(c) shows that image saturation detects the haze component in an input image.

Physical boundary of transmission is another informative feature for haze estimation. From (1), the lower bound of transmission t_l that ensures $0\leq\mathbf{J}\leq 1$ is given by

$$t_l=\max_{c\in\{r,g,b\}}\left(\max\left(\frac{A_c-I_c}{A_c},\frac{I_c-A_c}{1-A_c},\right)\right) \tag{2}$$

where subscript c denotes a color channel. Notice that we normalize pixel intensity values to be within $[0,1]$. As (2) constrains the solution space of transmission tightly, it has been adopted in the previous methods [20], [26], [27] to reduce inherent ambiguity of the dehazing problem. However, in practice, a small value of $1-A_c$ in the denominator where $I_c>A_c$ causes inadequate amplification of resultant t_l, making wrong estimation of transmission. To avoid small $1-A_c$ in the denominator, we replace it with A_c, then we have $I_{\text{low}}=\max_{c\in\{r,g,b\}}(|A_c-I_c|/A_c)$ as a final input feature. Figure 2(d) presents strong correlation of I_{low} with haze in the scene.

B. Function Set for Feature Assemble

Based on the previously defined input features in the terminal set, GP constructs an individual program in association with function operators. In addition to the basic operators such as arithmetic and mathematical ones, we define two types of special operators, namely channel operators and local operators, to extract single scalar values from input three-dimensional data. Note that these operators are applied in a successive manner and the order is not restricted.

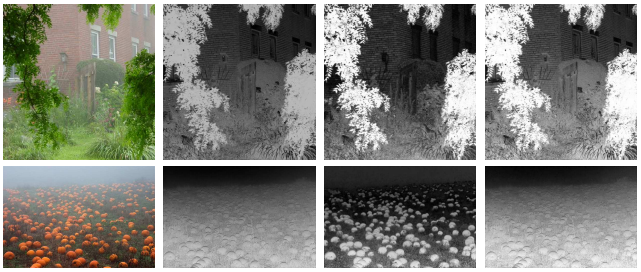

(a) (b) (c) (d)

Fig. 2. Candidate input features for terminal set. (a) hazy image $\mathbf{I}$, (b) green channel of $|\mathbf{I}-\mathbf{A}|$, (c) saturation I_{sat}, and (d) lower bound of transmission I_{low}.

For channel operators, we include max, min, and mean operators to aggregate pixel intensities across different color channels. In case of local operators, the median filter is additionally considered for its simplicity and efficiency. In [19], the median filter is applied to preserve edges with a low computational cost. Gibson et al. [28] have proposed MDCP (median dark channel prior) using the median filter to avoid halo effects during the regularization process. As the last local operator, we add the variance filter to capture characteristics of local blocks. As fog gets thick, pixel distribution is confined within a narrow dynamic range, which leads to low intensity variation. Therefore, the variance filter may be a good haze estimator by detecting local contrast. To take advantage of multi-scale processing, three scales of neighborhood $\mathcal{N}$ are employed for each local operator, e.g. 11×11, 13×13, and 15×15 patches.

IV. LEARNING TRANSMISSION MODEL

A. Preparing Training Data

Collecting good training data is a crucial task for most learning-based applications. In the proposed framework, pairs of observed hazy image $\mathbf{I}$ and corresponding transmission map t are required to train the model. However, unfortunately, a large scale of such data is extremely difficult to obtain especially in the outdoor environment since long range 3D depth is inaccurate, which demands time and labor consuming post-processing. Therefore, we synthesize hazy images from haze-free scenes, as employed in previous works [12], [14].

In contrast to the previous methods, we prepare training data in the more realistic scenario. First, haze-free images are obtained from the outdoor scene data. Specifically, we use two sets of data [29], [30] which include outdoor scenery that is likely to be degraded by haze. Then, we use uniformly distributed random transmission $t\in[t_{\min},1]$. We do not use extremely small t since it is not only physically invalid but also instable in the restoration procedure. $t_{\min}$ is fixed to $1/255$ in the preparation of training data. We also use random atmospheric light vector $\mathbf{A}$ based on the empirical distribution. In the conventional methods, $\mathbf{A}$ is fixed to a constant to reduce the uncertainty of variables in learning, and correlation across different color channels is not considered. In Figure 3, we plot the distribution of $\mathbf{A}$ over 75 benchmark hazy images using

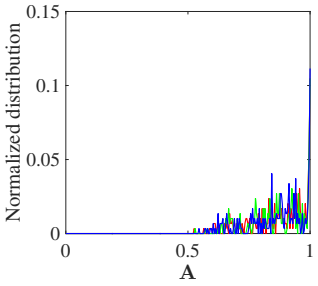

Fig. 3. Observed distribution of atmospheric light vector $\mathbf{A}$

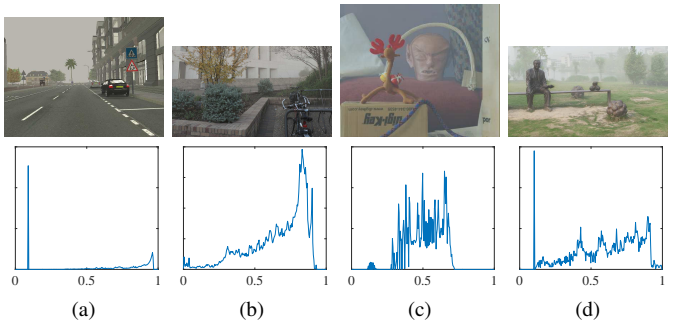

Fig. 4. Examples of hazy scene $\mathbf{I}$ and average distribution of transmission t for objective assessment: (a) FRIDA [32], (b) LIVE Color+3D [33], (c) Middlebury stereo [34]–[36], and (d) Fattal [37].

the method of [9]. We generate $\mathbf{A}$ based on this observed distribution.

Given haze-free image $\mathbf{J}$, atmospheric light vector $\mathbf{A}$, and transmission t, we finally obtain hazy scene $\mathbf{I}$. In our work, about 1,500 pictures are used to get one million sets of $(\mathbf{I}, \mathbf{A}, t)$ for the proposed learning architecture.

B. Scene Radiance Recovery by Learned Transmission Model

The objective of evolutionary methods is to maximize the performance of the individual program in terms of the fitness function. Fortunately, as we design the GP structure to estimate transmission directly, we simply determine the mean squared error between program output and ground-truth transmission value as a fitness function.

Then, from the GP result, we obtain the transmission model

$$\hat{t}(\mathbf{x}) = \alpha \left(\max_{\mathbf{y} \in \mathcal{N}(\mathbf{x})} I_{\text{low}}(\mathbf{y}) \right)^{\gamma} + \beta, \tag{3}$$

where I_{low} is a modified low bound of transmission in Table I, and $\alpha = 1.038$, $\beta = 0.07978$, and $\gamma = 0.5$ are learned parameters. Also, the largest scale, 15×15 block is selected as a neighborhood $\mathcal{N}$. This result suggests that I_{low} is the most informative feature for haze estimation. Moreover, I_{low} becomes identical to a pixel-wise DCP [9] when $A_c > I_c$. In other words, I_{low} is a more general form of DCP and an algebraic expression of it serves as a good estimator for haze in the scene.

So far, we have learned the transmission based on the assumption that the atmospheric light $\mathbf{A}$ is given. Therefore, it is required to estimate $\mathbf{A}$ to get an output transmission from the model. In [9], He et al. developed an estimation of $\mathbf{A}$, which reliably works in most outdoor scenes. Similarly, we calculate $\mathbf{A}$ by averaging pixel values of top 0.1% of scene points in the dark channel map.

Now, we obtain an initial transmission map via (3). Since a small transmission causes noise amplification, it is desirable to limit the range by setting the minimum value $t_{\min}$. However, it should be adaptively determined depending on each input image. We observe that the noise boosting frequently occurs where the initial transmission is small and the local patch has relatively low variance. As a result, $t_{\min}$ is empirically determined by the maximum value of initial transmission $\hat{t}(\mathbf{x})$ where local standard deviation and $\hat{t}(\mathbf{x})$ is less than 0.01 and 0.4, respectively. After applying the guided image filter [31] to refine the initial transmission, we finally obtain recovered scene radiance $\hat{\mathbf{J}}$ from (1).

V. Experimental Results

To verify the effectiveness of the proposed algorithm, we compare our results with five existing algorithms including dark channel prior (DCP) [9], no-black-pixel constraint (NBPC) [19], boundary constraint and contextual regularization (BCCR) [20], color attenuation prior (CAP) [14], and density of fog assessment-based defogger (DEFADE) [21]. We use authors' codes with default recommended settings to obtain the best results. For DCP, we implement it straightforwardly using the guided filter [31] to refine transmission.

We implement our method in MATLAB with GP toolbox GPTIPS [38]. We use standard settings in [25] except for the population size and the number of generations. In general, the larger population and the longer generation we define, the better solution we can potentially obtain. To strike balance between the computational cost and the performance, we set the population size and the number of generations as 200 and 70, respectively. As GP is a stochastic process, we run our method three times and select the best result. The total processing time for GP learning takes around 40 minutes.

A. Quantitative Assessment

We evaluate the performance of dehazing algorithms on four datasets: 1) foggy road image database (FRIDA) [32] with 18 urban road scenes, 2) LIVE Color+3D database [33] including 12 scenes with real depth acquired using an advanced range scanner, 3) 8 stereo images [34]–[36] with disparity maps, and 4) 14 images with ground-truth transmission map by Fattal [37]. Since these range data have different scales, we normalize and convert them to get a valid transmission map. Then, hazy scene $\mathbf{I}$ for the test is obtained via (1). To avoid that a specific $\mathbf{A}$ accidentally favors an algorithm, we synthesize test images with ten random $\mathbf{A}$ vectors and report an average score for each test scene. Examples of a hazy image and average distribution of transmission for each dataset are shown in Figure 4.

We assess dehazing performance objectively using three quality metrics, listed in Table II. First, we measure root mean squared error (RMSE) for all RGB pixel intensities

TABLE II
OBJECTIVE ASSESSMENT OF DEHAZING ALGORITHMS USING FOUR METRICS: RMSE, EUC LAB, COLOR CORRELATION, AND COMPUTATION TIME. FOR EACH RESULT, THE BEST AND THE SECOND BEST ARE BOLDFACED AND UNDERLINED, RESPECTIVELY.

Metric	Set	DCP	NBPC	BCCR	CAP	DEFADE	Proposed
RMSE	1	0.184	0.169	0.148	0.129	0.147	**0.114**
	2	0.173	0.173	0.162	0.124	0.178	**0.120**
	3	**0.113**	0.170	0.118	0.122	0.142	0.119
	4	0.149	0.166	0.145	0.128	0.183	**0.120**
	avg	0.155	0.169	0.143	0.126	0.163	**0.118**
EUC LAB	1	19.065	20.915	17.283	14.143	16.573	**12.189**
	2	15.245	19.759	14.799	10.310	17.734	**9.772**
	3	12.168	21.234	13.080	12.196	17.283	**11.908**
	4	13.914	21.335	14.242	12.705	20.537	**11.197**
	avg	15.098	20.811	14.851	12.339	18.032	**11.266**
Color Corr.	1	0.887	0.797	0.912	0.923	**0.942**	0.940
	2	0.761	0.684	0.760	0.844	0.784	**0.848**
	3	0.904	0.780	0.878	0.920	0.902	**0.924**
	4	0.866	0.795	0.866	0.878	0.838	**0.884**
	avg	0.855	0.764	0.854	0.891	0.866	**0.899**
time	avg	5.066	**3.628**	10.488	3.892	87.145	5.434

between reconstructed $\hat{\mathbf{J}}$ and ground-truth radiance $\mathbf{J}$. Second, we compare an average Euclidean distance of pixels in LAB color space. It is known that perceptual difference between two colors coincide with Euclidean distance in LAB color [39]. Third, we evaluate an average RGB correlation between $\hat{\mathbf{J}}$ and $\mathbf{J}$. The proposed algorithm provides the best objective scores in most datasets. DCP shows good performance, particularly on the third dataset. From this result, we can see that DCP is a reliable estimator for a mid-ranged transmission. CAP also exhibits remarkable performance, but the proposed algorithm is superior for all datasets.

Additionally, we analyze the computational complexities of the dehazing algorithms to process one million pixels, as compared in Table II. We use a personal computer with a 2.2-GHz CPU. The proposed algorithm achieves average computation speed among the competitors, but it can be accelerated by optimization.

B. Qualitative Assessment

In this section, we provide examples of output images to assess their qualities subjectively and analyze the characteristics of the proposed algorithm in comparison with those of the existing algorithms. Figure 5 compares the restoration results on six hazy images. Both DCP and BCCR show good performance on the overall test data. However, these approaches tend to yield suppressed transmission, which leads to brightness reduction and noise amplification in the recovered scene. Processed images by NBPC suffer from color distortion due to the wrong estimation of transmission and the simplified regularization process. DEFADE conveys clear visual perception in its results, but also causes contrast overstretching, making information loss in the darkened region. CAP yields almost identical results to those of the proposed method since both algorithms are learning based. However, as verified in the previous section, the proposed algorithm provides quantitatively better performance.

VI. CONCLUSION

We proposed a GP-based learning methodology to discover a robust feature representation for image dehazing. We considered the feature learning task as a combinatorial optimization problem, and used GP to solve automatically through candidate features and a group of primitive operators. We found that transmission can be formulated as a simple algebraic expression in terms of the haze-relevant input features. Experimental results demonstrated that the proposed algorithm effectively removes haze on both synthetic and real-world images.

REFERENCES

[1] S. G. Narasimhan and S. K. Nayar, "Contrast restoration of weather degraded images," *IEEE Trans. Pattern Anal. Mach. Intell.*, vol. 25, no. 6, pp. 713–724, Jun. 2003.

[2] Y. Y. Schechner, S. G. Narasimhan, and S. K. Nayar, "Polarization-Based Vision Through Haze," *Applied Optics*, vol. 42, no. 3, p. 511, 2003.

[3] L. Schaul, C. Fredembach, and S. Susstrunk, "Color image dehazing using the near-infrared," in *Proc. IEEE ICIP*, Nov. 2009, pp. 1629–1632.

[4] J. Kopf, B. Neubert, B. Chen, M. Cohen, D. Cohen-Or, O. Deussen, M. Uyttendaele, and D. Lischinski, "Deep photo: Model-based photograph enhancement and viewing," in *ACM Trans. Graph.*, vol. 27, no. 5, Dec. 2008, p. 116.

[5] S. G. Narasimhan and S. K. Nayar, "Interactive (de) weathering of an image using physical models," in *IEEE Workshop on Color and Photometric Methods in Computer Vision*, vol. 6, no. 6.4. France, 2003, pp. 1–8.

[6] N. Hautiére, J.-P. Tarel, J. Lavenant, and D. Aubert, "Automatic fog detection and estimation of visibility distance through use of an onboard camera," *Machine Vision and Applications*, vol. 17, no. 1, pp. 8–20, Jan. 2006.

[7] R. Tan, "Visibility in bad weather from a single image," in *Proc. IEEE CVPR*, Jun. 2008, pp. 1–8.

[8] R. Fattal, "Single image dehazing," in *ACM Trans. Graph.*, vol. 27, no. 3, Aug. 2008, p. 72.

[9] K. He, J. Sun, and X. Tang, "Single Image Haze Removal Using Dark Channel Prior," *IEEE Trans. Pattern Anal. Mach. Intell.*, vol. 33, no. 12, pp. 2341–2353, Dec. 2011.

[10] K. B. Gibson, S. J. Belongie, and T. Q. Nguyen, "Example based depth from fog," in *Proc. IEEE ICIP*, Sep. 2013, pp. 728–732.

[11] W. Freeman, T. Jones, and E. Pasztor, "Example-based super-resolution," *IEEE Computer Graphics and Applications*, vol. 22, no. 2, pp. 56–65, Mar. 2002.

[12] K. Tang, J. Yang, and J. Wang, "Investigating haze-relevant features in a learning framework for image dehazing," in *Proc. IEEE CVPR*, 2014, pp. 2995–3002.

[13] L. Breiman, "Random forests," *Machine learning*, vol. 45, no. 1, pp. 5–32, 2001.

[14] Q. Zhu, J. Mai, and L. Shao, "A Fast Single Image Haze Removal Algorithm Using Color Attenuation Prior," *IEEE Trans. Image Process.*, vol. 24, no. 11, pp. 3522–3533, Nov. 2015.

[15] R. Poli, "Genetic programming for image analysis," in *Proceedings of the 1st Annual Conference on Genetic Programming*. MIT Press, 1996, pp. 363–368.

[16] R. d. S. Torres, A. X. Falcão, M. A. Gonçalves, J. P. Papa, B. Zhang, W. Fan, and E. A. Fox, "A genetic programming framework for content-based image retrieval," *Pattern Recognition*, vol. 42, no. 2, pp. 283–292, 2009.

[17] R. A. Davis, A. J. Charlton, S. Oehlschlager, and J. C. Wilson, "Novel feature selection method for genetic programming using metabolomic 1 H NMR data," *Chemometrics and Intelligent Laboratory Systems*, vol. 81, no. 1, pp. 50–59, 2006.

(a) (b) (c) (d) (e) (f) (g)

Fig. 5. Dehazing results on the test images: “NY12,” “NY17,” “Canyon,” “girls,” “people,” and “mountain”: (a) input hazy image, (b) DCP [9], (c) NBPC [19], (d) BCCR [20], (e) CAP [14], (f) DEFADE [21], and (g) the proposed algorithm.

[18] L. Liu, L. Shao, X. Li, and K. Lu, “Learning spatio-temporal representations for action recognition: A genetic programming approach,” *IEEE Trans. on Cybern.*, vol. 46, no. 1, pp. 158–170, 2016.

[19] J.-P. Tarel and N. Hautiére, “Fast visibility restoration from a single color or gray level image,” in *Proc. IEEE ICCV*, Sep. 2009, pp. 2201–2208.

[20] G. Meng, Y. Wang, J. Duan, S. Xiang, and C. Pan, “Efficient image dehazing with boundary constraint and contextual regularization,” in *Proc. IEEE ICCV*, Dec. 2013, pp. 617–624.

[21] L. K. Choi, J. You, and A. Bovik, “Referenceless Prediction of Perceptual Fog Density and Perceptual Image Defogging,” *IEEE Trans. Image Process.*, vol. 24, no. 11, pp. 3888–3901, Nov. 2015.

[22] E. J. McCartney, “Optics of the atmosphere: scattering by molecules and particles,” *New York, John Wiley and Sons, Inc.*, vol. 1, 1976.

[23] W. E. K. Middleton, “Vision through the Atmosphere.” University of Toronto Press. Toronto, Canada, 1952.

[24] M. Sulami, I. Glatzer, R. Fattal, and M. Werman, “Automatic recovery of the atmospheric light in hazy images,” in *Proc. IEEE ICCP*, 2014, pp. 1–11.

[25] R. Poli, W. B. Langdon, and N. F. McPhee, *A field guide to genetic programming*, 2008.

[26] J.-H. Kim, W.-D. Jang, J.-Y. Sim, and C.-S. Kim, “Optimized contrast enhancement for real-time image and video dehazing,” *J. Vis. Commun. Image Represent.*, vol. 24, no. 3, pp. 410–425, Apr. 2013.

[27] Y.-H. Lai, Y.-L. Chen, C.-J. Chiou, and C.-T. Hsu, “Single-Image Dehazing via Optimal Transmission Map Under Scene Priors,” *IEEE Trans. Circuits Syst. Video Technol.*, vol. 25, no. 1, pp. 1–14, Jan. 2015.

[28] K. B. Gibson, D. T. Vo, and T. Q. Nguyen, “An investigation of dehazing effects on image and video coding,” *IEEE Trans. Image Process.*, vol. 21, no. 2, pp. 662–673, 2012.

[29] S. Gould, R. Fulton, and D. Koller, “Decomposing a scene into geometric and semantically consistent regions,” in *Proc. IEEE ICCV*, 2009, pp. 1–8.

[30] S. Wang, J. Joo, Y. Wang, and S.-C. Zhu, “Weakly supervised learning for attribute localization in outdoor scenes,” in *Proc. IEEE CVPR*, 2013, pp. 3111–3118.

[31] K. He, J. Sun, and X. Tang, “Guided Image Filtering,” *IEEE Trans. Pattern Anal. Mach. Intell.*, vol. 35, no. 6, pp. 1397–1409, Jun. 2013.

[32] J.-P. Tarel, N. Hautiére, L. Caraffa, A. Cord, H. Halmaoui, and D. Gruyer, “Vision enhancement in homogeneous and heterogeneous fog,” *IEEE Intell. Transp. Syst. Mag.*, vol. 4, no. 2, pp. 6–20, 2012.

[33] C. C. Su, L. K. Cormack, and A. C. Bovik, “Color and depth priors in natural images,” *IEEE Trans. Image Process.*, vol. 22, no. 6, pp. 2259–2274, June 2013.

[34] D. Scharstein and R. Szeliski, “High-accuracy stereo depth maps using structured light,” in *Proc. IEEE CVPR*, vol. 1, 2003, pp. I–195.

[35] D. Scharstein and C. Pal, “Learning conditional random fields for stereo,” in *Proc. IEEE CVPR*, 2007, pp. 1–8.

[36] H. Hirschmüller and D. Scharstein, “Evaluation of cost functions for stereo matching,” in *Proc. IEEE CVPR*, 2007, pp. 1–8.

[37] R. Fattal, “Dehazing using color-lines,” *ACM Trans. Graph.*, vol. 34, no. 1, p. 13, 2014.

[38] D. P. Searson, “GPTIPS 2: an open-source software platform for symbolic data mining,” in *Handbook of Genetic Programming Applications*. Springer, 2015, pp. 551–573.

[39] A. K. Jain, *Fundamentals of Digital Image Processing*. Prentice Hall, Inc., 1989.